JGR Atmospheres

Key Points:

- A refined approach to estimate nitrogen oxides emissions for isolated cities using wind fields and satellite nitrogen dioxide data
- Many sampling boxes defined for each city, increasing success of deriving emissions from 40% to 60% for one box to 100% for 54 boxes
- Applied to 19 cities in South and Southeast Asia to estimate annual emissions of 22–181 kilotonnes in 2019

Author Contributions:

Conceptualization: Gongda Lu, Eloise A. Marais
Data curation: Gongda Lu, Karn Vohra
Formal analysis: Gongda Lu, Eloise A. Marais
Funding acquisition: Eloise A. Marais
Investigation: Gongda Lu, Eloise A. Marais, Karn Vohra, Rebekah P. Horner, Dandan Zhang, Randall V. Martin, Sarath Guttikunda
Methodology: Gongda Lu, Eloise A. Marais, Randall V. Martin
Project administration: Gongda Lu, Eloise A. Marais
Resources: Rebekah P. Horner, Dandan Zhang

Near-Automated Estimate of City Nitrogen Oxides Emissions Applied to South and Southeast Asia

Gongda Lu[1], Eloise A. Marais[1] ![ORCID], Karn Vohra[1] ![ORCID], Rebekah P. Horner[1] ![ORCID], Dandan Zhang[2], Randall V. Martin[2] ![ORCID], and Sarath Guttikunda[3,4] ![ORCID]

[1]Department of Geography, University College London, London, UK, [2]Department of Energy, Environmental, and Chemical Engineering, Washington University in St. Louis, St. Louis, MO, USA, [3]Transportation Research and Injury Prevention (TRIP) Center, Indian Institute of Technology, New Delhi, India, [4]Urban Emissions, New Delhi, India

Abstract Cities in South and Southeast Asia are developing rapidly without routine, up-to-date knowledge of air pollutant precursor emissions. This data deficit can potentially be addressed for nitrogen oxides (NO_x) by deriving city NO_x emissions from satellite observations of nitrogen dioxide (NO_2) sampled under windy conditions. NO_2 plumes of isolated cities are aligned along a consistent wind-rotated direction and a best-fit Gaussian is applied to estimate emissions. This approach currently relies on non-standardized choice of upwind, downwind, and across-wind distances from the city center, resulting in fits that often fail or yield non-physical parameters. Here, we propose an automated approach that defines many combinations of distances yielding 54 distinct sampling boxes that we test with TROPOspheric Monitoring Instrument (TROPOMI) NO_2 observations over 19 isolated cities in South and Southeast Asia. Our approach is efficient, uses open-source software, is adaptable to many cities, standardizes and eliminates sensitivity to sampling box choice, increases success of deriving emissions from 40% to 60% with one sampling box to 100% (all 19 cities) with 54, and yields emissions consistent with the current manual approach. We estimate that the annual emissions range from 15 ± 5 mol s^{-1} for Bangalore (India) to 125 ± 41 mol s^{-1} for Dhaka (Bangladesh). With enhanced success of deriving top-down emissions, we find support from comparison to past studies and inventory estimates that top-down emissions may be biased, as the method does not adequately account for spatial and seasonal variability in NO_x photochemistry. Further methodological development is needed for enhanced accuracy and use to derive sub-annual emissions.

Plain Language Summary Cities are a large source of nitrogen oxides (NO_x) that go on to form many types of air pollutants of harm to human health. City NO_x emissions estimated with observations from space-based instruments are vital in regions that lack access to up-to-date, locally developed inventories. Success of obtaining satellite-derived emissions hinges on user selection of a sampling box around each city center. Here we present an automated, efficient method that uses many (54) boxes. When tested on 19 cities in South and Southeast Asia, annual NO_x emissions are obtained for all 19 cities compared to about half the selected cities when using a single sampling box. With this updated approach, we estimate total NO_x emissions in 2019 that range from 22 kilotonnes for Bangalore to almost 10-times more (181 kilotonnes) for Dhaka. The greater success of our updated approach also helps us identify that the accuracy of emissions derivation from satellite observations should be further improved by accounting for the influence of spatial and seasonal variability in NO_x photochemistry.

1. Introduction

Nitrogen oxides ($NO_x \equiv NO_2 + NO$) react to form particulate nitrate and tropospheric ozone and deposit to sensitive habitats (Luo et al., 2019; Sillman, 1999), thus degrading air quality, altering climate, and adversely affecting human health and the environment (Grulke & Heath, 2020; Lelieveld et al., 2015; Marais et al., 2023; Yue et al., 2017). Controls targeting anthropogenic sources of NO_x have been extensively implemented in cities in Europe, the US and China (Curier et al., 2014; de Foy et al., 2016; Silvern et al., 2019). In cities in other parts of the world, particularly South and Southeast Asia, NO_x is increasing rapidly due to fast economic development and limited or absent air quality policies (Vohra et al., 2021, 2022). Vohra et al. (2022) used 14 years of satellite observations of NO_2 from the Ozone Monitoring Instrument (OMI) to infer increases of ~1–14% a^{-1} in surface NO_2 pollution in almost all rapidly developing large cities in South and Southeast Asia. Only in Jakarta did NO_2 decline due to emission controls applied to vehicles (Vohra et al., 2022). Population projections suggest that, by

Software: Gongda Lu
Supervision: Eloise A. Marais
Validation: Gongda Lu
Visualization: Gongda Lu, Eloise A. Marais
Writing – original draft: Gongda Lu, Eloise A. Marais
Writing – review & editing: Gongda Lu, Eloise A. Marais, Karn Vohra, Rebekah P. Horner, Dandan Zhang, Randall V. Martin, Sarath Guttikunda

2100, one-fifth of the world's most populous cities will be in Southeast Asia (Hoornweg & Pope, 2017), necessitating reliable and up-to-date NO_x emissions estimates for assessing the impact of this growth on urban air quality and for informing air quality policies.

Bottom-up inventories provide estimates of anthropogenic NO_x emissions, but publicly available versions for South and Southeast Asia do not adequately represent contemporary local conditions, as these are derived using outdated activity data, are resource-intensive to produce so lag the present day, have only recently been updated to achieve spatial resolutions that resolve cities, and the activity and emission factor data needed to compile the inventories are lacking for many countries (Kurokawa & Ohara, 2020). The two most used bottom-up inventories for these regions are the Regional Emission inventory in Asia (REAS) (Kurokawa & Ohara, 2020) and the inventory known as MIX, a mosaic of REAS and other regional inventories (Li et al., 2017). REAS and the first version of MIX (MIXv1) are at ∼25 km resolution, MIXv1 only covers 2 years of data, and the most recent years are 2015 for REAS and 2010 for MIXv1. A new version of MIX (MIXv2) recently developed covers more years (2010–2017) and better resolves (∼10 km resolution) emissions than MIXv1 (Li et al., 2024), though most widely used global inventories, such as the Community Emissions Data System (CEDS$_{GBD-MAPS}$) (McDuffie et al., 2020) and Hemispheric Transport of Air Pollution (HTAP) (Crippa et al., 2023), still rely on REAS and MIXv1.

Independent and contemporary estimates of city NO_x emissions can be derived with satellite observations of tropospheric NO_2 vertical column densities (VCDs) without the need to simulate computationally intensive models to convert VCDs to emissions. A method first proposed by Beirle et al. (2011) involves selecting isolated cities and treating these as large point sources of NO_x. In this approach, individual satellite pixels within a target domain centered on a city center were split into eight major wind directions to resolve the city plume in each direction. A model was then fit to the plume to account for its Gaussian shape and for exponential decay of NO_x. This fit, referred to as an Exponential Modified Gaussian (EMG), yields parameters that are then used to estimate NO_x emissions. It also yields an effective lifetime of NO_x for the city plume that is dominated by dispersion for the windy conditions sampled. As dispersion dominates, the derived lifetime is much shorter than the chemical lifetime of NO_x that includes conversion to nitric acid (HNO_3) or organic nitrates (de Foy et al., 2014; Laughner & Cohen, 2019) and, to a lesser extent, dry deposition of NO_2 (Zhang et al., 2012). Beirle et al. (2011) used OMI observations of NO_2 to derive NO_x emissions for eight global megacities. The Beirle et al. (2011) approach required many (four) years of OMI data to achieve distinct plumes in each wind direction.

Valin et al. (2013) expanded on the approach developed by Beirle et al. (2011) by demonstrating that all satellite data can instead be aligned along a single upwind-downwind direction relative to the city center. This approach reduced the number of observations needed to distribute the data by wind direction and so extended application to a greater number of geographically isolated cities over shorter sampling periods. Wind rotation of OMI observations and the EMG fit have since been used to calculate city NO_x emissions predominantly in the US (de Foy et al., 2014; Goldberg, Lu, Oda, et al., 2019; Lu et al., 2015) and for select cities worldwide (Goldberg et al., 2021). Following the 2017 launch of the higher spatial resolution TROPOspheric Monitoring Instrument (TROPOMI), the wind rotation, EMG fit, and related approaches have been extended to smaller isolated cities and shorter sampling periods than was possible with OMI. Applications include cities in western Europe (Lorente et al., 2019; Pommier, 2023; Pope et al., 2022), China (Wu et al., 2021), the US (Goldberg, Lu, Streets, et al., 2019), and worldwide (Lange et al., 2022), as well as investigating changes in NO_x emissions due to COVID-19 lockdown measures in the New York Metropolitan Area (Tzortziou et al., 2022) and in select cities in India, Argentina, and Spain (Lange et al., 2022). So far, the wind rotation and EMG fit has only been applied to 5–13 cities in South and Southeast Asia as part of global studies (Goldberg et al., 2021; Lange et al., 2022).

There has been substantial development in the use of satellite observations to derive emissions of isolated hotspots which can improve the EMG fit with wind rotation, such as automated hotspot detection and selection (Beirle et al., 2021; McLinden et al., 2016). Still, users need to define a sampling box around the city that effectively captures the wind rotated plume, requiring trial and error selection of a single suitable sampling box (Laughner & Cohen, 2019) that typically varies with city size and plume length (Goldberg, Lu, Oda, et al., 2019; Lange et al., 2022; Lu et al., 2015). Even after selecting a suitable sampling box, the EMG fit is often poor or yields non-physical best-fit parameters (Laughner & Cohen, 2019), decreasing the likelihood of deriving top-down
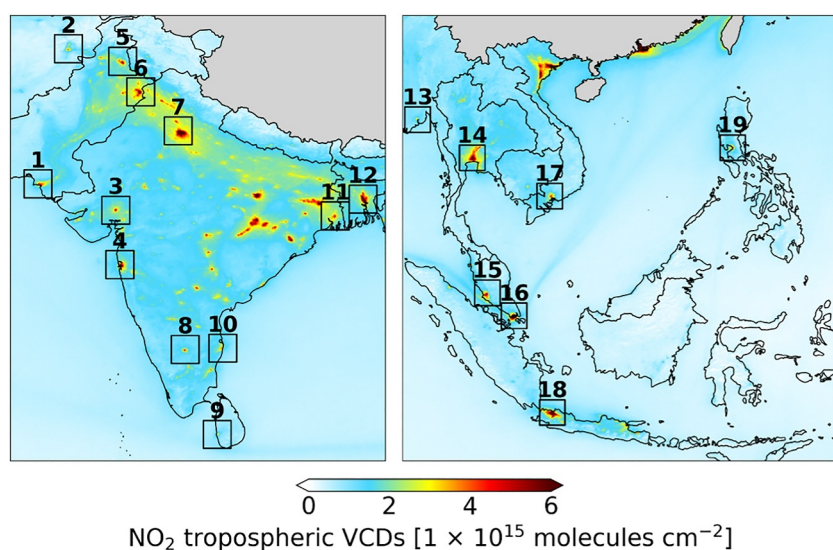
Figure 1. Annual mean TROPOMI tropospheric NO_2 vertical column densities over South and Southeast Asia in 2019. Maps show South (left) and Southeast (right) Asia TROPOMI NO_2 oversampled to $0.05° \times 0.05°$. The 19 selected cities, numbered from east to west, are Karachi (1), Islamabad (5), and Lahore (6) in Pakistan; Kabul (2) in Afghanistan; Ahmedabad (3), Mumbai (4), Delhi (7), Bangalore (8), Chennai (10), and Kolkata (11) in India; Colombo (9) in Sri Lanka; Dhaka (12) in Bangladesh; Yangon (13) in Myanmar; Bangkok (14) in Thailand; Kuala Lumpur (15) in Malaysia; the sovereign city Singapore (16); Ho Chi Minh City (17) in Vietnam; Jakarta (18) in Indonesia; and Manila in the Philippines (19).

emissions. Selecting appropriate city-specific boxes for the wide-ranging city sizes in South and Southeast Asia is also time consuming and not standardized.

Here we develop a near-automated and efficient EMG fitting routine for deriving annual city NO_x emissions, demonstrate the utility of this automation by applying it to TROPOMI NO_2 observations over isolated cities in South and Southeast Asia with wide-ranging city sizes, compare our top-down emissions to past studies and a global bottom-up inventory, and exploit the greater success of our updated sampling to identify opportunities to further develop and improve the EMG fit approach.

2. Materials and Methods

2.1. TROPOMI NO_2 and City Selection

We use Level 2 TROPOMI NO_2 tropospheric column VCDs for 2019 from the Sentinel-5P Products Algorithm Laboratory (S5P-PAL) portal (https://data-portal.s5p-pal.com/; last acquired 30 January 2022). These data have been retrieved with a consistent algorithm (version 02.03.01) that corrects for a low bias in NO_2 over polluted scenes (Eskes et al., 2021). TROPOMI achieves daily global coverage with a swath width of 2,600 km, an equator crossing time of 13:30 local solar time (LST), and a nadir pixel resolution that increased on 5 August 2019 from $7\ km \times 3.5\ km$ to $5.5\ km \times 3.5\ km$. We use cloud-free, high-quality data identified with a quality flag ≥ 0.75 (van Geffen et al., 2021).

To identify isolated cities appropriate for top-down estimate of NO_x emissions, we first oversample TROPOMI NO_2 to obtain high-resolution gridded annual means ($0.05° \times 0.05°$; ~6 km latitude × ~5 km longitude) by weighting areas of overlap between the satellite pixels and cells on a fixed latitude-longitude grid using tessel-lation (Sun et al., 2018). We use the resultant gridded TROPOMI NO_2 shown in Figure 1 to manually select 19 cities that are isolated hotspots. The 19 selected cities are Karachi, Islamabad, and Lahore in Pakistan; Kabul in Afghanistan; Ahmedabad, Mumbai, Delhi, Bangalore, Chennai, and Kolkata in India; Colombo in Sri Lanka; Dhaka in Bangladesh; Yangon in Myanmar; Bangkok in Thailand; Kuala Lumpur in Malaysia; the sovereign city Singapore; Ho Chi Minh City in Vietnam; Jakarta in Indonesia; and Manila in the Philippines. The other prominent enhancements in Figure 1 we do not select are either not cities, such as the coal-fired power plants concentrated in eastern India, or are not isolated, such as the cluster of cities (Hanoi, Haiphong and Nam Dinh) in northern Vietnam.
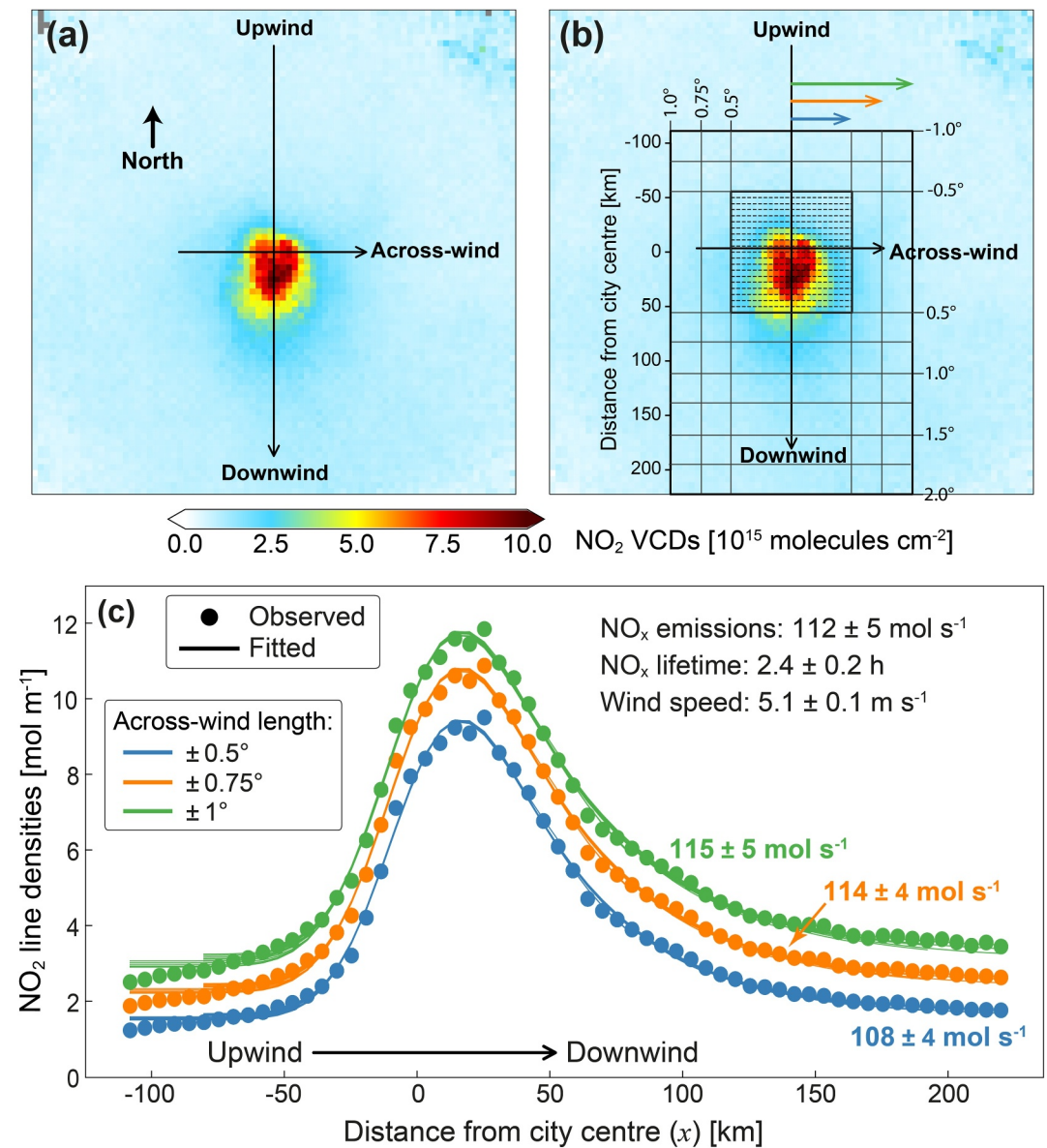
Figure 2. Illustration of major steps in the wind rotation and Exponential Modified Gaussian (EMG) fit to derive annual nitrogen oxides (NO$_x$) emissions for Singapore. The main steps in each panel are wind rotate and grid windy scene TROPOMI NO$_2$ pixels to 0.05° × 0.05° (a), fill data gaps (b), and fit the EMG function (Equation 1) (solid lines) to observed line densities (filled circles) (c). The 8 gray grid squares in panel (a) indicate missing data. In panel (b), black rectangles show the extent of the largest (1° upwind, 2.0° downwind, and 1.0° across wind) and smallest (0.5° upwind, downwind and across wind) sampling boxes, gray lines demarcate sampling box edges, dashed lines in the smallest box show the 0.05° increments used to calculate the line densities in panel (c), and colored arrows correspond to the across-wind integration lengths in panel (c). All 54 successful EMG fits, 18 lines for each of the 3 across-wind lengths, are shown in panel (c). Values in panel (c) give the mean and standard deviation of NO$_x$ emissions (Equation 3) for all 54 fits and for the 18 fits for each of the 3 across-wind lengths, the effective NO$_x$ lifetime for all fits (Equation 2), and the sampling box mean ERA5 wind speed. The goodness-of-fit (R^2) is ≥0.99 for all fits in panel (c).

2.2. Wind Rotation and EMG Fit

Figure 2 illustrates the major steps involved in the wind rotation and EMG fit to derive annual NO$_x$ emissions for Singapore. The wind fields we use to calculate wind direction and speed to retain TROPOMI NO$_2$ observations under windy conditions are the fifth generation European ReAnalysis (ERA5) 3D hourly u and v wind components (https://cds.climate.copernicus.eu/cdsapp#!/home; last acquired 18 March 2022) provided at 0.25° × 0.25°

resolution. At each TROPOMI NO_2 pixel, we compute collocated mean ERA5 wind speeds and directions 30 min around 13:30 LST, the TROPOMI overpass time, in the lowest 5 layers ($\geq$900 hPa) to capture dispersion of mixed-layer near-surface NO_2 plumes. Within a 4° × 4° domain around each city center, we isolate TROPOMI pixels with coincident wind speeds >2 m s^{-1}, the threshold typically used for windy conditions (Beirle et al., 2011; Pope et al., 2022). We rotate each TROPOMI NO_2 pixel by the angle of its wind direction, preserving the distance of the pixel from the city center. Wind rotation aligns all pixels along the same "upwind-downwind" direction that in our work is from north to south (Figure 2a) and displaces any nearby sources so that these appear as rings a fixed distance from the city center (Fioletov et al., 2016). Examples of these include the two hotspots, Lahore and Delhi (Figure 1), that have small NO_2 enhancements north of the city. As a result of this displacement by wind rotation, these hotspots are not incorporated in the city plume. After wind rotating all pixels in a year, we grid pixels onto a uniform 0.05° × 0.05° grid using simple point-in-box averaging (Figure 2a) and fill empty grid cells (gray squares in Figure 2a) using nearest-neighbor interpolation to reduce low biases in the steps that follow. For most cities, there are very few empty grid cells (8 for Singapore in Figure 2a) and the empty grid cells typically occur at the outer edges of the domain.

Next, line densities or NO_2 integrated along the across-wind direction are calculated by summing grid cells in Figure 2b in the across-wind (east-to-west) direction in 0.05° upwind-downwind (north-to-south) increments. In the standard approach, a single box smaller than the 4° × 4° domain is used, defined by the distance upwind, downwind, and across-wind of the city center. Instead of using a single box, we define multiple boxes that encompass the range of sizes typically used in past studies (Goldberg et al., 2021; Lange et al., 2022; Laughner & Cohen, 2019). These, defined as degree distances from the city center, are 0.5°, 0.75°, and 1° upwind, 0.5°, 0.75°, 1.0°, 1.25°, 1.5°, 1.75°, 2.0° downwind, and 0.5°, 0.75°, and 1.0° across-wind. This combination of 3 upwind, 7 downwind and 3 across-wind lengths yields 63 boxes and associated line densities, decreasing to 54 to satisfy the requirement that the distance downwind of the city center be $\geq$ the distance upwind to encompass the downwind extent of the city plume. The sizes of the smallest and largest boxes, the extent of all other sampling boxes, and the across-wind 0.05° increments summed to obtain line densities in the smallest box are shown in Figure 2b.

The EMG model we use to fit to the observed 1D line densities in each sampling box is the Laughner and Cohen (2019) formulation:

$$F\left(x\,|\,a,x_0,\mu_x,\sigma_x,B\right) = \frac{a}{2x_0}\exp\left(\frac{\mu_x}{x_0} + \frac{\sigma_x^2}{2x_0^2} - \frac{x}{x_0}\right)\mathrm{erfc}\left(-\frac{1}{\sqrt{2}}\left[\frac{x-\mu_x}{\sigma_x} - \frac{\sigma_x}{x_0}\right]\right) + B \qquad (1)$$

where x is the distance of each line density upwind and downwind of the city center (Figure 2c) and a, x_0, μ_x, σ_x, and B are best-fit parameters. Of these, a is total NO_2 in the plume (in moles), x_0 is the e-folding distance or length scale of NO_2 decay (in km), μ_x is the location of the apparent source relative to the city center (in km) or upwind edge of the plume that in Figure 2c is located ~5 km upwind or north of the city center, σ_x is the Gaussian smoothing length scale (in km) that is ~40% of the Full Width at Half Maximum (FWHM/2.355), and B is background NO_2 (in mol m^{-1}). In the rare instances there are small NO_2 enhancements nearby target hotspots (Delhi and Lahore; Figure 1), displacement of these by wind rotating the city plume limits the contribution of these enhancements to the background, B.

We use initial guesses for the best-fit parameters in Equation 1 that are similar to those used by Laughner and Cohen (2019) for US cities, but our fitting procedure differs. Laughner and Cohen (2019) used a non-linear interior point minimization algorithm (the *fmincon* function in MATLAB) to optimize model parameters. Instead, we perform the fit with the open source *scipy.optimize.curve_fit* module from SciPy Python package version 1.7.3, as is used by Pommier (2023) for hotspots in the UK. Laughner and Cohen (2019) performed 10 iterative fits and selected the fit with the smallest residuals. We instead iterate on the fit until the difference in fitting parameters between the current and previous iteration is negligible (<0.001%) for at most 10 iterations. Fit convergence is usually achieved after three iterations, resulting in a fast fitting routine. We only retain good-quality fits, identified with goodness-of-fits (R^2) > 0.8, as in Laughner and Cohen (2019). We further screen for physically implausible best-fit parameters using criteria similar to Laughner and Cohen (2019): a is positive, x_0 is at least 1.6 km (approximately 1/e of the grid resolution), μ_x is within the sampling box, the emission width is less than the e-folding distance ($\sigma_x < x_0$), background NO_2 is positive and less than the maximum line density

value, the e-folding distance occurs between the plume center and the edge of the sampling box, and that 1.5 times μ_x is less than the downwind length.

The Singapore example in Figure 2 is an ideal city, as all 54 EMG fits succeed. Figure S1 in Supporting Information S1 shows the wind rotated plume, line densities and EMG fits for an example city, Bangalore, with 15 failed fits, necessitating as many as 54 sampling boxes. The first criteria these fits fail to satisfy are $R^2 > 0.8$ for 14 fits and $a > 0$ mol for 1 of the fits. Figure 2c and Figure S1 in Supporting Information S1 show that the observed line densities are most sensitive to the across-wind length, as this determines the amount of NO_2 summed to yield each line density. All sampling boxes encompass the Bangalore plume, whereas sampling boxes with a downwind length $>1°$ are required to encompass the whole Singapore plume.

The successful EMG fits are used to calculate effective NO_x lifetimes (τ_{NO_x}; reported in h) and midday NO_x emissions (E_{NO_x}; in mol s^{-1}):

$$\tau_{NO_x} = \frac{x_0}{\omega} \tag{2}$$

$$E_{NO_x} = \gamma \times \frac{a}{\tau_{NO_x}} \tag{3}$$

where ω is the sampling box mean wind speed (in m s^{-1}) and γ is the city mean midday molar ratio of $[NO_x]/[NO_2]$ required to convert moles NO_2 to moles NO_x. The up to 54 individual estimates of τ_{NO_x} and E_{NO_x} are averaged to obtain values for each city.

We use the same $[NO_x]/[NO_2] = 1.32$ value as Beirle et al. (2011) and subsequent studies to represent rapid cycling between NO and NO_2. Liu et al. (2022) determined with synthetic experiments that city NO_x emissions are relatively unaffected by variability in $[NO_x]/[NO_2]$, but that study was for US cities. Surface measurements aid in determining suitability of $[NO_x]/[NO_2] = 1.32$, but these are limited to cities in India and have data quality issues (Vohra et al., 2021). Instead, we use the GEOS-Chem model to assess suitability of the 1.32 value. We simulate the model in 2019 and sample the lowest model layer around the TROPOMI overpass time. We use output from a coarse and finer resolution version of GEOS-Chem to also test sensitivity of this ratio to model resolution, especially given many of these cities are coastal (Figure 1). We use the classical configuration of the model that operates on a single computational node, called GEOS-Chem Classic (GCClassic), and the high-performance model configuration (GCHP) that is parallelized across multiple computational nodes to enable finer resolution global simulations (Eastham et al., 2018). GCClassic is version 13.3.4 (https://doi.org/10.5281/zenodo.5764874) run on a fixed 2° × 2.5° global grid and GCHP is version 13.4.1 (https://doi.org/10.5281/zenodo.6564711) run on a C360 global grid (~25 km × ~25 km), the finest global GEOS-Chem grid resolution full-year simulation achieved to date. GCClassic and GCHP use the same vertical grid and chemical mechanism. For GCClassic, grid squares that overlap with each city are sampled, whereas for GCHP, we use city sampling extents determined from a combination of administrative and geographic boundary shapefiles and Google Maps (Figure S2 in Supporting Information S1). Midday sampling is at 12:00 to 15:00 LST from GCClassic and 13:00 to 14:00 LST from GCHP. At midday, NO_x is in photochemical steady state, so the relative abundance of NO and NO_2 is insensitive to differences in these sampling windows (Potts et al., 2021).

We calculate uncertainties in the NO_x emissions by adding individual errors in quadrature. These include best-fit parameters x_0 and a, sampling box mean wind speed ω, the TROPOMI NO_2 observations, and $[NO_x]/[NO_2]$. We use the relative standard deviation from all successful EMG fits to calculate city-specific errors in x_0 and a. For ω, we consider errors due to the choice of spatial and temporal sampling and the threshold used for windy conditions. We use the Beirle et al. (2011) estimated 10% error in temporal sampling choice and 5% error due to vertical sampling choice. We conduct our own tests of the sensitivity to wind speed threshold and spatial sampling choice. For $[NO_x]/[NO_2]$ we assess whether the 10% error attributed to this variable by Beirle et al. (2011) is appropriate by quantifying the percent deviation of GCClassic and GCHP $[NO_x]/[NO_2]$ from 1.32. Beirle et al. (2011) applied a 30% error to OMI that is also appropriate for TROPOMI. Even though uncertainties in TROPOMI slant columns (NO_2 along the viewing path) are much less than those from OMI (van Geffen et al., 2020), the air mass factor used to convert slant columns to VCDs remains the largest contributor to errors in NO_2 VCDs and is similar for OMI and TROPOMI (van Geffen et al., 2021).

We benchmark our approach by comparing our NO_x emissions to top-down NO_x emissions obtained using a single sampling box. The studies we consider are those using satellite observations for the same time period as ours. These include multiyear (2017–2019) mean emissions from Goldberg et al. (2021) obtained using the OMI sensor and emissions from Lange et al. (2022) obtained with select days of TROPOMI data from 2018 to 2020.

2.3. Bottom-Up Anthropogenic Emissions

We compare our top-down estimates to anthropogenic NO_x emissions from the widely used bottom-up HTAP inventory version 3 (HTAP_v3) (Crippa et al., 2023). HTAP_v3 downscales the REAS $0.25° \times 0.25°$ emissions to $0.1° \times 0.1°$ using sector-specific spatial fields (https://www.cmascenter.org/sa-tools/; last accessed 2 July 2024) to resolve emissions from underlying urban activities like residential combustion and road traffic. The most recent HTAP_v3 emission year is 2018, achieved by extending emissions from the regional REAS inventory ending in 2015 to the year 2018 with trends from the Emissions Database for Global Atmospheric Research (EDGAR) inventory. The same sampling boundaries as GCHP are used (Section 2.2; Figure S2 in Supporting Information S1). The HTAP_v3 NO_x emissions include contributions from aviation, transport (road, rail, pipeline, inland waters), shipping, energy, industry, and residential sectors.

Cities targeted can be influenced by non-anthropogenic NO_x sources, such as open burning of biomass (Marvin et al., 2021) and natural sources such as soils (Weng et al., 2020) and lightning (Miyazaki et al., 2014). We assess suitability of comparing our top-down emissions to anthropogenic bottom-up emissions only by determining the percent contribution of anthropogenic emissions to total NO_x emissions. To do this, we simulate total NO_x emissions with the Harmonized Emissions Component (HEMCO) standalone model version 3.0.0 (https://zenodo.org/records/4984639; last accessed 20 March 2022) (Lin et al., 2021) and sample the same spatial extent as GCHP and HTAP_v3 (Figure S2 in Supporting Information S1). HEMCO is run at a spatial resolution of $0.25° \times 0.3125°$ (~28 km latitude $\times$ ~33 km longitude). HEMCO calculates open biomass burning emissions using the Global Fire Emissions Database with small fires (GFED4s) inventory (Randerson et al., 2017) and reads in and processes lightning and soil NO_x from offline emissions at the same resolution as HEMCO (Murray et al., 2012; Weng et al., 2020).

Bottom-up emissions from HTAP_v3 are 24-hr means, whereas top-down estimates derived using TROPOMI are representative of midday emissions. Goldberg et al. (2021) multiplied satellite-derived midday NO_x emissions by 0.77 to convert midday top-down NO_x emissions to 24-hr means for comparison to bottom-up inventories. This value was inferred from bottom-up emissions estimates for the Netherlands, so may not be suitable for the selected cities in South and Southeast Asia. The hourly scaling factors used by HEMCO for the chosen cities range from 0.70 to 1.16. These are for the year 2000 and are extrapolations of values for conditions in Europe, so may not be suitable for the year and cities targeted in this study. Given this, we do not scale top-down emissions and instead discuss whether differences in averaging times contribute to discrepancies between top-down and bottom-up emissions estimates.

3. Results and Discussion

3.1. Wind Rotation and EMG Fit Metrics

The enhancement apparent due north of Lahore (city (6) in Figure 1) is deflected by wind rotation as an evenly distributed ring ~200 km away from the city center, causing a small second peak that only influences boxes with the longest downwind length of 2°. The emissions estimate for the boxes with the longest downwind lengths is 35.3 ± 1.8 mol s^{-1}, just 3% more than the mean of all successful fits (34.2 ± 1.6 mol s^{-1}). The enhancement north of Delhi (city (7) in Figure 1) causes multiple uneven rings, but most of these are deflected northeast of the city beyond the sampling boxes.

The line densities generated (shown in Figure 2c for Singapore) are obtained by summing NO_2 over ~100 km for the blue lines, ~150 km for the orange lines, and ~200 km for the green lines. As is evident in Figure 2c, an increase in across-wind length causes a systematic increase in the line densities. The background, B, almost doubles, from 1.7 mol m^{-1} for the $\pm 0.5°$ across-wind length to 3.2 mol m^{-1} for $\pm 1.5°$, but the total NO_2 in the plume, a, is relatively similar. Values of a for Singapore are 66.4 ± 1.7 mol for $\pm 0.5°$ across-wind fits, 74.7 ± 2.6 mol for $\pm 1°$, and 78.7 ± 3.5 mol for $\pm 1.5°$. NO_x emissions increase by just 6% from 108 mol s^{-1} at $\pm 0.5°$ to 115 mol s^{-1} at $\pm 1.5°$.
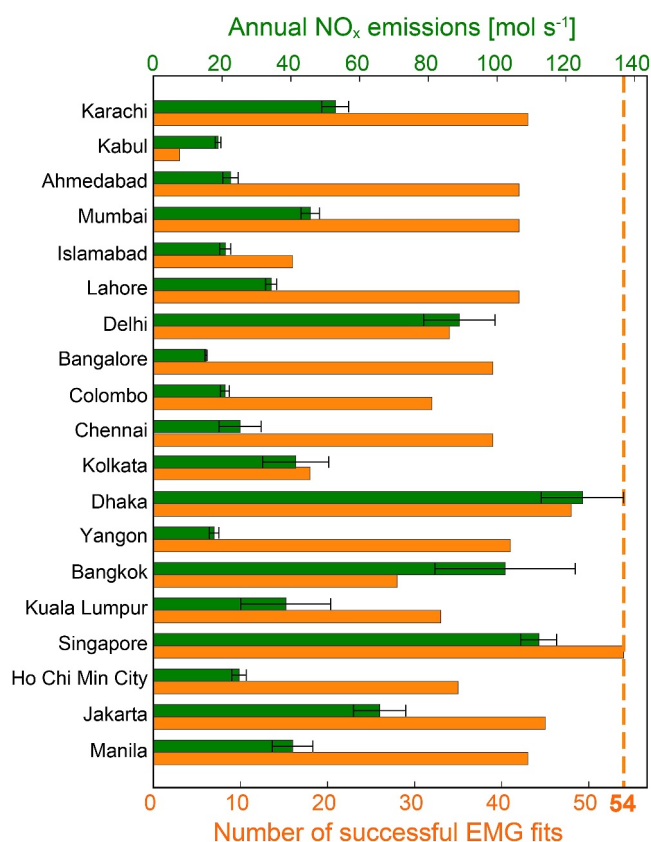
Figure 3. Successful Exponential Modified Gaussian (EMG) fits and top-down nitrogen oxides emissions for the cities targeted in this study. Bars are emissions (green) and the corresponding number of successful fits (orange). Black error lines are the EMG fit error for each city obtained as the standard deviation of all successful fits. The orange dashed line at 54 indicates the maximum possible EMG fits. Emissions multiplied by ~1.45 yields emissions in Gg NO_2 a^{-1}.

Isolating satellite pixels coincident with windy conditions (>2 m s^{-1}) removes 8%–34% of all 2019 quality- and cloud-screened TROPOMI NO_2 pixels for most cities in Figure 1. Cities with greater data loss are Lahore (43% data loss), Kabul (58%) and Islamabad (63%). No spatial data gap filling (Section 2.2, Figure 2) is needed within the boxes sampled, due to the high sampling frequency of TROPOMI. If only a single domain size is selected, annual EMG fits meet all criteria for success for 7 to 12 of the 19 cities in Figure 1, depending on the sampling box chosen. Using our extended method, we successfully derive annual NO_x emissions for all 19 cities, due to the enhanced probability of obtaining at least one successful EMG fit.

Figure 3 shows the number of successful EMG fits (orange bars) range from 3 (Kabul) to all 54 (Singapore). Singapore, Dhaka, Jakarta, Karachi, Manila, and Mumbai are least impacted by sampling box choice. The 4 cities, Kabul, Islamabad, Kolkata and Bangkok, with <30 fits are most likely to fail if only a single sampling box is used. For all retained EMG fits, differences between observed and fitted NO_2 line densities, the fit residuals, are always negligible. The most common causes for a failed EMG fit rank as: $R^2 \leq 0.8$ (24%), emission width > e-folding distance (19%), total plume NO_2 (a in Equation 1) < 0 (13%), and e-folding distance > the downwind length of the sampling box (12%).

We also test sensitivity of top-down NO_x emissions to the choice of wind speed threshold and horizontal sampling extent to attribute an error to these. For this, we apply a stricter wind speed threshold of 3 m s^{-1} and test the difference in NO_x emissions if instead of filtering for windy conditions using pixel-mean wind fields, we calculate a sampling-box mean wind speed to filter for windy conditions as in Goldberg, Lu, Oda, et al. (2019). We apply these conditions to a mid-sized sampling box of 0.75° upwind, 1.5° downwind, and ±0.75° across-wind. Variability in NO_x emissions for cities with successful EMG fits for all 4 wind sampling conditions is at most 10% (Figure S3 in Supporting Information S1). Given these results, we attribute a 10% error to the choice of horizontal sampling and to the wind speed threshold.

GCClassic (coarse resolution) annual mean [NO_x]/[NO_2] for the target cities ranges from 1.25 (Dhaka) to 1.41 (Kabul). The range in ratios from GCHP (finer resolution) is wider at 1.24 (Ahmedabad) to 1.64 (Kolkata). The difference in ratios between the coarse and fine resolution models is typically ±10%, except for a few cities with ratios from the fine resolution model that exceed the coarse resolution model by 14% for Singapore, 16% for Lahore, 23% for Dhaka, and 23% for Kolkata. This is because the fine resolution model better resolves the city plume that includes a greater proportion of NO_x as NO from fresh emission sources. As the difference between the model city ratios and the 1.32 value is ±10% for most cities, we use the same 10% error for [NO_x]/[NO_2] as Beirle et al. (2011).

3.2. Top-Down NO_x Emissions

Green bars in Figure 3 show the mean annual top-down NO_x emissions for all cities. These range from ~15 mol s^{-1} for Bangalore to ~125 mol s^{-1} for Dhaka. The range in the total mass of NO_x emitted for these cities, assuming the midday emission rate is reasonably representative of the 24-hr emission rate, is 22–181 Gg NO_x as NO_2. Emissions for most cities are <50 mol s^{-1} (<73 Gg NO_x as NO_2 a^{-1}). Cities with emissions between 50 and 100 mol s^{-1} (73–145 Gg NO_x as NO_2 a^{-1}) include Karachi, Delhi, and Jakarta and >100 mol s^{-1} (>145 Gg NO_x as NO_2 a^{-1}) include Bangkok, Singapore, and Dhaka. Emission rates for Bangkok, Dhaka and Singapore are comparable to the range of top-down emissions estimated for large, polluted cities in China also obtained with the EMG approach (Wu et al., 2021). The effective lifetimes for the cities in Figure 1 (shown in Figure S4 in Supporting Information S1) range from 1.2 hr for Colombo to 6.2 hr for Kuala Lumpur. Variability in effective lifetimes depends most strongly on the downwind extent of the plume. The Pearson's correlation coefficient, R, between city mean effective lifetimes and x_0 (decay length scale) is 0.89.

For most of the target cities, the variability in NO_x emissions for individual successful EMG fits is small (black error lines in Figure 3). Relative standard deviations of annual NO_x emissions range from just 2% for Bangalore to 34% for Kuala Lumpur and are <15% for most (16 out of 19) cities. This variability is far less than the equivalent Gaussian fit uncertainty of 10%–50% estimated by Beirle et al. (2011) for a single sampling box. The relatively large variability in Kuala Lumpur NO_x emissions is because the smaller EMG sampling boxes do not fully encompass the elongated wind rotated city NO_2 plume, causing a lower estimate in NO_x emissions for the smaller boxes compared to the larger boxes sampled. The effect of this is dampened by the almost 30 successful fits used to obtain mean NO_x emissions for this city. The relative standard deviations of the effective NO_x lifetimes (Figure S4 in Supporting Information S1) range from 6% for Bangalore to 37% for Chennai. The relative standard deviations of other parameters are <6% for wind speeds (Figure S5 in Supporting Information S1), 5% (Bangalore) to 38% (Chennai) for x_0, and 4% (Kabul) to 41% (Kuala Lumpur) for a.

The overall uncertainty in annual NO_x emissions we obtain by adding the fit errors (error lines in Figure 3) and all other error contributions in quadrature, as detailed in Section 2.2, ranges from 32% for Kabul to 59% for Kuala Lumpur. Mean emissions and total errors for all cities are given in Table S1 in Supporting Information S1. The TROPOMI NO_2 VCDs make the largest contribution to the overall uncertainty. The higher-end of our uncertainty estimates is similar to the typical ∼50% uncertainty reported in past studies (Beirle et al., 2011; Goldberg et al., 2021; Verstraeten et al., 2018).

The accuracy of the top-down emissions in Figure 3 should ideally be determined by comparison to true emissions from reliable ground-based observations, but these are non-existent. An alternate approach is to conduct synthetic experiments with GEOS-Chem to assess the accuracy of the wind rotation and EMG method, but the model is too coarse to resolve the city plume shape shown in Figure 2c, affecting the best-fit parameter estimates. Given these limitations, we instead evaluate consistency with city NO_x emissions estimates from past studies that used wind rotation and the EMG fit and from the HTAP inventory. We use our overall uncertainties (Table S1 in Supporting Information S1) in the comparison to past studies and HTAP in the sections that follow.

3.3. Comparison to Top-Down Estimates From Past Studies

To assess our approach, we compare in Figure 4 our annual NO_x emissions to values from past studies that used similar sampling time periods and a single sampling box. These include multiyear (2017–2019) mean emissions from Goldberg et al. (2021) obtained using the OMI sensor and emissions from Lange et al. (2022) obtained with select days of TROPOMI data from 2018 to 2020. Goldberg et al. (2021) estimated emissions for 10 of the 19 cities in our study. These we read from their Figure S10 in Supporting Information S1 for Karachi, Figure S11 in Supporting Information S1 for 4 cities in India, and Figure S13 in Supporting Information S1 for 5 cities in Southeast Asia and divide by the 0.77 midday to 24-hr scaling factor used in that study. Emissions are reported by Lange et al. (2022) for 5 of the 19 cities in our study. Based on the regression statistics in Figure 4, our emissions are typically ∼25% more than estimates from these past studies. Exceptions are Mumbai, Ahmedabad, and Chennai that in our study are 16%–29% less than Goldberg et al. (2021). Lange et al. (2022) used an earlier version of the TROPOMI data product that has a known low bias in NO_2 VCDs over very polluted scenes (van Geffen et al., 2022). Differences in TROPOMI data products are the likely cause for our higher Delhi (by 27%) and Singapore (by 18%) emissions. Relatively small error estimates from Lange et al. (2022) are because they only propagate error contributions from the wind speed data and the EMG fit.

Discrepancies between Goldberg et al. (2021) and our emissions are most likely dominated by differences in wind fields. When we apply our approach to the same OMI data product and the same time period as Goldberg et al. (2021) (2017–2019), we obtain emissions estimates that differ by <20% from our TROPOMI emissions values in Table S1 in Supporting Information S1 for 14 of the 18 cities that we succeed in obtaining emissions with OMI. Goldberg et al. (2021) used ERA5 wind fields at 100 m that would have slower average wind speeds than the surface to 900 hPa averaged wind fields we use (Section 2.2). Emissions have been shown to increase with increase in wind speed by as much as 15% using winds sampled at 500 m compared to at 100 m for a sensitivity test by Goldberg et al. (2022) for Dallas, Texas. Sampling box choice may also be a factor. For example, the smallest of our 54 boxes yields NO_x emissions of 102 mol s^{-1} for Singapore that is 10 mol s^{-1} less than the mean of all EMG fits. Sampling period may be an issue too, though just for Delhi and Karachi. As these cities are north of 25°N, only May–September observations were used by Goldberg et al. (2021). We find that Delhi and Karachi mean May–September TROPOMI NO_2 VCDs in 2019 averaged within the 4° × 4° domain
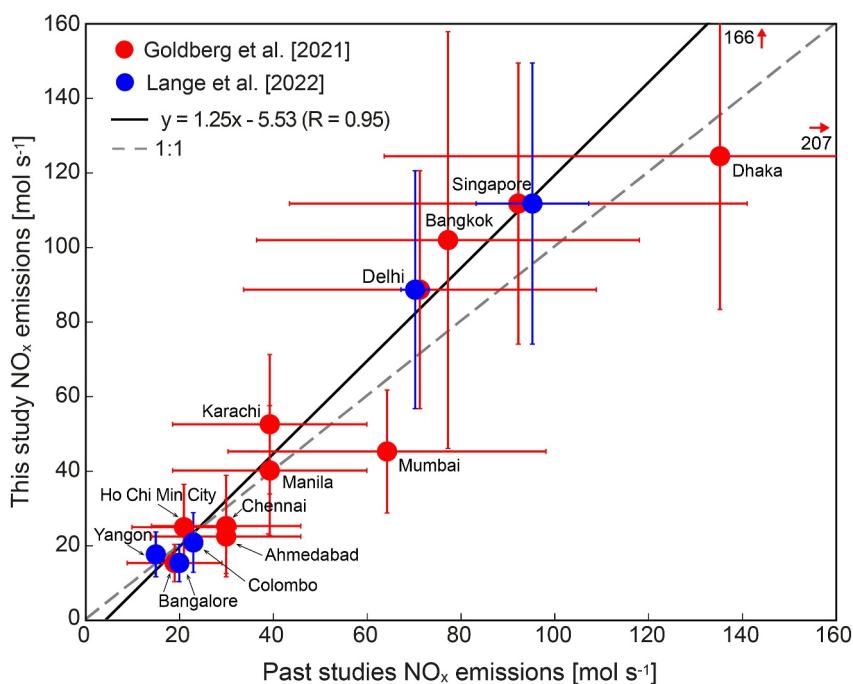
Figure 4. Comparison of our and past top-down nitrogen oxides emissions. Symbols compare our emissions to those from Goldberg et al. (2021) (red) and Lange et al. (2022) (blue). Error bars are overall uncertainties for our study (Section 2.2, Table S1 in Supporting Information S1), the same 53% uncertainty applied to all cities by Goldberg et al. (2021) and the city-specific uncertainties for Lange et al. (2022). Lines are the Theil regression fit (solid black) and 1:1 relationship (dashed gray). Inset text gives the regression statistics and Pearson's correlation coefficient (R). Arrows and inset text for Dhaka give the error values that extend beyond the plotting range.

selected for each city (Figures 2a and 2b) are 11%–12% less than those in October–April, due to the shorter photochemical lifetime of NO_x in the warmer months. Open biomass burning emissions also influence seasonality in the TROPOMI NO_2 VCDs, but the EMG fit accounts for this by distinguishing background NO_2 (B in Equation 1) from NO_2 in the city plume (a in Equation 1).

We find that if we apply the EMG fit to individual months for Delhi and Karachi, all 54 EMG fits fail for Delhi in July–August and yield spurious results in September due to large data loss resulting from persistent clouds during the monsoon season. All 12 months are retained for Karachi, Singapore and Manila. November–April mean values of a are 21% more than in May–October for Karachi, 9% more for Singapore, and 39% more for Manila. This suggests that using NO_2 VCDs for a portion of the year may yield systematic biases in emissions that may not reflect seasonality in the underlying activities affecting the emissions. Larger wintertime than summertime emissions have also been reported in the global study of Lange et al. (2022). They quantified summer-to-winter emission ratios of ∼0.5 for Colombo and Delhi. The top-down emissions calculation (Equation 3) does not fully account for seasonality in photochemistry. The derived effective NO_x lifetimes used to calculate NO_x emissions (Equation 2) are mostly influenced by dispersion. As a result, the effective lifetimes are much shorter than the expected chemical lifetimes of NO_x (de Foy et al., 2014). In the synthetic experiment scenarios tested by de Foy et al. (2014), the EMG fit applied to wind rotated data yielded an effective lifetime of 4 hr for a 12-hr chemical lifetime scenario. According to Shah et al. (2020), the chemical lifetime of NO_x for central-eastern China centered at ∼35°N, the northerly portion of our domain, ranges from ∼6 hr in summer to ∼24 hr in winter. None of the monthly effective lifetimes for our target cities reproduce this seasonality and the longest lifetime is 12.7 ± 1.8 hr for Lahore in June. The implication is that the size of absolute emissions derived with sub-annual satellite data may be biased, but should have negligible effect if used to quantify relative trends, as in Goldberg et al. (2021) and Laughner and Cohen (2019), for example.
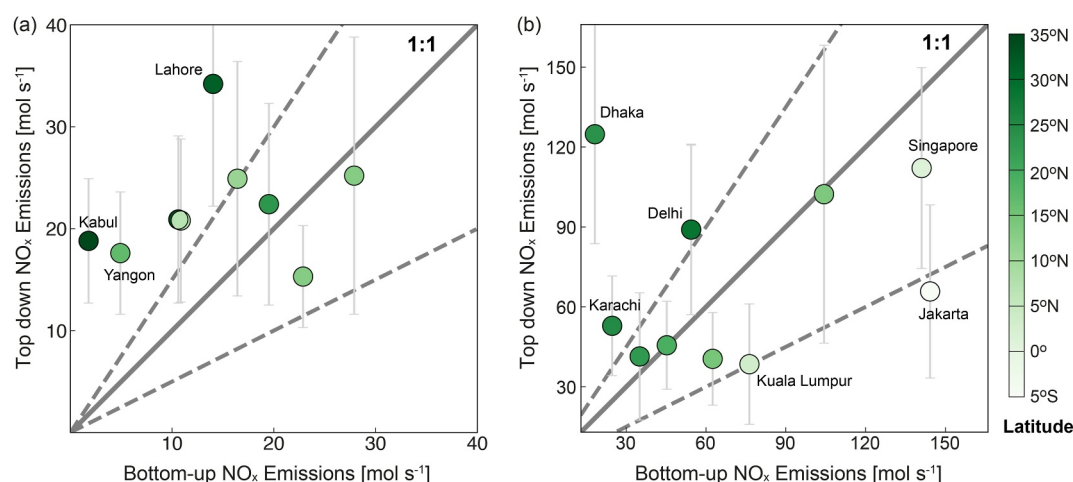
Figure 5. Comparison of annual top-down and bottom-up nitrogen oxides (NO_x) emissions for target cities. Data are colored by city center latitude and split into top-down NO_x emissions <35 mol s^{-1} (a) and ≥ 35 mol s^{-1} (b). Error bars are the overall uncertainty in top-down emissions estimates. Gray lines indicate 1:1 agreement (solid) and $\pm 50\%$ difference (dashed). The bottom-up emissions sampling extent of each city is in Figure S2 in Supporting Information S1. Data used to generate the figure are in Table S1 in Supporting Information S1.

3.4. Comparison to Bottom-Up Emissions

Figure 5 compares annual top-down and bottom-up NO_x emissions. According to our HEMCO simulations, anthropogenic sources account for most ($>87\%$) annual NO_x emissions. The relative differences between our top-down estimates and the bottom-up inventory are within 50% for Mumbai ($<1\%$), Bangkok (2%), Chennai (10%), Ahmedabad (15%), Kolkata (18%), Singapore (21%), Bangalore (33%), and Manila (35%). A 50%–100% difference occurs for Kuala Lumpur (50%), Ho Chi Minh City (52%), Jakarta (54%), Delhi (64%), and Colombo (92%). Even greater relative differences occur for Islamabad (2 times), Karachi (2.1 times), Lahore (2.4 times), Yangon (3.6 times), Dhaka (6.9 times), and Kabul (11-fold). The largest absolute discrepancies are for Dhaka and Jakarta. Bottom-up emissions are 107 mol s^{-1} less than the top-down values for Dhaka and 78 mol s^{-1} more for Jakarta. On a mass basis, this is equivalent to a 155 Gg NO_x as NO_2 underestimate for Dhaka and a 113 Gg NO_x as NO_2 overestimate for Jakarta.

The different years used (2018 for HTAP, 2019 for TROPOMI) should at most account for a 14% difference in emissions, based on the size of annual trends inferred by Vohra et al. (2022) using long-term observations of OMI NO_2 VCDs over large and fast-growing cities in South and Southeast Asia. Vohra et al. (2022) identified that emission inventories do not capture the steep decline in NO_x emissions in Jakarta attributed to national policies targeting vehicles. In addition to misrepresenting annual changes in underlying activities, the emission factors are mostly informed by studies of China and Japan (Kurokawa & Ohara, 2020). The bottom-up and top-down emissions differences for many cities also exceed the $\pm 30\%$ difference that results from the choice of bottom-up emissions grid sampling and the $\pm 30\%$ difference from the timing of the top-down (midday) and bottom-up (24-hr) estimates inferred by Goldberg et al. (2021).

Even though there are large uncertainties and biases in bottom-up emissions, a latitudinal pattern in the discrepancies is apparent in Figure 5. Top-down emissions are greater than bottom-up emissions for cities to the north and vice versa for cities to the south, so that in general top-down emissions exceed bottom-up emissions in South Asia and vice versa in Southeast Asia. NO_x chemical loss varies with latitude, due to variability in the amount of sunlight available to form hydroxyl and peroxy radicals required to form HNO_3 and organic nitrates, the main daytime chemical loss pathway for NO_x. This latitudinal pattern is likely because the EMG fit does not fully account for spatial variability in NO_x photochemistry, imparting a bias in the top-down emissions. The size of this bias will depend on the relative contribution of NO_x chemical loss to total loss in the wind rotated plume. The latitudinal pattern occurs even if instead of using the same $[NO_x]/[NO_2]$ of 1.32, we use city-specific $[NO_x]/[NO_2]$ from GCHP (Figure S6 in Supporting Information S1).

4. Conclusions

City NO_x emissions can be derived with a now well-established approach using satellite observations of nitrogen dioxide (NO_2), wind rotation and a Gaussian fit to the city plume. Issues with this approach are that the choice of sampling box around the city center is not standardized and so is prone to subjective box selection and the Gaussian fit often fails or yields non-physical best-fit parameters. Here we address these issues by applying 54 sampling boxes to isolated cities. We test our method with TROPOspheric Monitoring Instrument (TROPOMI) NO_2 observations for 2019 over 19 large, isolated cities in South and Southeast Asia that lack contemporary, publicly available bottom-up emissions estimates. Our approach offers advantages over the single sampling box approach of being faster, more automated, more successful, and yielding city-specific error estimates of best-fit parameters.

Annual NO_x emissions, obtained for all 19 cities, are <73 Gg NO_x as NO_2 a^{-1} for most cities, between 73 and 145 Gg NO_x as NO_2 a^{-1} for Karachi, Delhi, and Jakarta and >145 Gg NO_x as NO_2 a^{-1} for Bangkok, Dhaka, and Singapore. The overall uncertainty in the annual emissions is 30%–60%. Our NO_x emissions estimates are strongly correlated ($R = 0.95$) with values from past studies, with explainable differences that are due to differences in satellite data products, wind fields, and months targeted. The latter we suggest may lead to biases, as the top-down emissions estimate does not properly account for seasonality in photochemical loss of NO_x. Relative differences between our top-down estimates and a widely used bottom-up inventory are <50% for 8 of the 19 cities, within 50%–100% for Kuala Lumpur, Ho Chi Minh City, Jakarta, Delhi, and Colombo, and much greater for Karachi (2.1 times), Islamabad (2.1 times), Lahore (2.4 times), Yangon (3.3 times), Dhaka (6.9 times), and Kabul (11-fold). There is a latitudinal dependence of the size of these discrepancies that we suggest is because the top-down approach does not properly account for spatial variability in the chemical lifetime of NO_x.

The increased success of deriving NO_x emissions with our updated approach enables us to identify that further development is needed to account for time and space variability in the chemical lifetime of NO_x to fully exploit the top-down approach to interrogate seasonality in emissions, to validate bottom-up emissions, to exploit hourly observations from geostationary instruments, and to inform air quality regulation.

Conflict of Interest

The authors declare no conflicts of interest relevant to this study.

Data Availability Statement

The TROPOMI tropospheric columns for 2019 are publicly available from the S5P-PAL Data Portal (https://data-portal.s5p-pal.com/). GEOS-Chem source codes are preserved on Zenodo by The International GEOS-Chem User Community (2021) for GCClassic version 13.3.4 and by The International GEOS-Chem User Community (2022) for GCHP version 13.4.1.

References

Beirle, S., Boersma, K. F., Platt, U., Lawrence, M. G., & Wagner, T. (2011). Megacity emissions and lifetimes of nitrogen oxides probed from space. *Science*, *333*(6050), 1737–1739. https://doi.org/10.1126/science.1207824

Beirle, S., Borger, C., Dörner, S., Eskes, H., Kumar, V., de Laat, A., & Wagner, T. (2021). Catalog of NO_x emissions from point sources as derived from the divergence of the NO_2 flux for TROPOMI. *Earth System Science Data*, *13*(6), 2995–3012. https://doi.org/10.5194/essd-13-2995-2021

Crippa, M., Guizzardi, D., Butler, T., Keating, T., Wu, R., Kaminski, J., et al. (2023). The HTAP_v3 emission mosaic: Merging regional and global monthly emissions (2000-2018) to support air quality modelling and policies. *Earth System Science Data*, *15*(6), 2667–2694. https://doi.org/10.5194/essd-15-2667-2023

Curier, R. L., Kranenburg, R., Segers, A. S., Timmermans, R. M. A., & Schaap, M. (2014). Synergistic use of OMI NO_2 tropospheric columns and LOTOS-EUROS to evaluate the NO_x emission trends across Europe. *Remote Sensing of Environment*, *149*, 58–69. https://doi.org/10.1016/j.rse.2014.03.032

de Foy, B., Lu, Z. F., & Streets, D. G. (2016). Satellite NO_2 retrievals suggest China has exceeded its NO_x reduction goals from the twelfth Five-Year Plan. *Scientific Reports*, *6*, 9. https://doi.org/10.1038/srep35912

de Foy, B., Wilkins, J. L., Lu, Z. F., Streets, D. G., & Duncan, B. N. (2014). Model evaluation of methods for estimating surface emissions and chemical lifetimes from satellite data. *Atmospheric Environment*, *98*, 66–77. https://doi.org/10.1016/j.atmosenv.2014.08.051

Eastham, S. D., Long, M. S., Keller, C. A., Lundgren, E., Yantosca, R. M., Zhuang, J., et al. (2018). GEOS-chem high performance (GCHP v11-02c): A next-generation implementation of the GEOS-Chem chemical transport model for massively parallel applications. *Geoscientific Model Development*, *11*(7), 2941–2953. https://doi.org/10.5194/gmd-11-2941-2018

Eskes, H., van Geffen, J., Sneep, M., Veefkind, P., Niemeijer, S., & Zehner, C. (2021). S5P Nitrogen Dioxide v02.03.01 intermediate reprocessing on the S5P-PAL system: Readme file.

Fioletov, V. E., McLinden, C. A., Krotkov, N., Li, C., Joiner, J., Theys, N., et al. (2016). A global catalogue of large SO_2 sources and emissions derived from the Ozone Monitoring Instrument. *Atmospheric Chemistry and Physics*, *16*(18), 11497–11519. https://doi.org/10.5194/acp-16-11497-2016

Goldberg, D. L., Anenberg, S. C., Lu, Z. F., Streets, D. G., Lamsal, L. N., McDuffie, E. E., & Smith, S. J. (2021). Urban NO_x emissions around the world declined faster than anticipated between 2005 and 2019. *Environmental Research Letters*, *16*(11), 11. https://doi.org/10.1088/1748-9326/ac2c34

Goldberg, D. L., Harkey, M., de Foy, B., Judd, L., Johnson, J., Yarwood, G., & Holloway, T. (2022). Evaluating NO_x emissions and their effect on O_3 production in Texas using TROPOMI NO_2 and HCHO. *Atmospheric Chemistry and Physics*, *22*(16), 10875–10900. https://doi.org/10.5194/acp-22-10875-2022

Goldberg, D. L., Lu, Z. F., Oda, T., Lamsal, L. N., Liu, F., Griffin, D., et al. (2019). Exploiting OMI NO_2 satellite observations to infer fossil-fuel CO_2 emissions from US megacities. *Science of the Total Environment*, *695*, 9. https://doi.org/10.1016/j.scitotenv.2019.133805

Goldberg, D. L., Lu, Z. F., Streets, D. G., de Foy, B., Griffin, D., McLinden, C. A., et al. (2019). Enhanced capabilities of TROPOMI NO_2: Estimating NO_x from north American cities and power plants. *Environmental Science & Technology*, *53*(21), 12594–12601. https://doi.org/10.1021/acs.est.9b04488

Grulke, N. E., & Heath, R. L. (2020). Ozone effects on plants in natural ecosystems. *Plant Biology*, *22*(S1), 12–37. https://doi.org/10.1111/plb.12971

Hoornweg, D., & Pope, K. (2017). Population predictions for the world's largest cities in the 21st century. *Environment and Urbanization*, *29*(1), 195–216. https://doi.org/10.1177/0956247816663557

Kurokawa, J., & Ohara, T. (2020). Long-term historical trends in air pollutant emissions in Asia: Regional Emission inventory in ASia (REAS) version 3. *Atmospheric Chemistry and Physics*, *20*(21), 12761–12793. https://doi.org/10.5194/acp-20-12761-2020

Lange, K., Richter, A., & Burrows, J. P. (2022). Variability of nitrogen oxide emission fluxes and lifetimes estimated from Sentinel-5P TROPOMI observations. *Atmospheric Chemistry and Physics*, *22*(4), 2745–2767. https://doi.org/10.5194/acp-22-2745-2022

Laughner, J. L., & Cohen, R. C. (2019). Direct observation of changing NO_x lifetime in North American cities. *Science*, *366*(6466), 723–727. https://doi.org/10.1126/science.aax6832

Lelieveld, J., Evans, J. S., Fnais, M., Giannadaki, D., & Pozzer, A. (2015). The contribution of outdoor air pollution sources to premature mortality on a global scale. *Nature*, *525*(7569), 367–371. https://doi.org/10.1038/nature15371

Li, M., Kurokawa, J., Zhang, Q., Woo, J.-H., Morikawa, T., Chatani, S., et al. (2024). MIXv2: A long-term mosaic emission inventory for Asia (2010–2017). *Atmospheric Chemistry and Physics*, *24*(7), 3925–3952. https://doi.org/10.5194/acp-24-3925-2024

Li, M., Zhang, Q., Kurokawa, J., Woo, J. H., He, K. B., Lu, Z. F., et al. (2017). MIX: A mosaic Asian anthropogenic emission inventory under the international collaboration framework of the MICS-Asia and HTAP. *Atmospheric Chemistry and Physics*, *17*(2), 935–963. https://doi.org/10.5194/acp-17-935-2017

Lin, H. P., Jacob, D. J., Lundgren, E. W., Sulprizio, M. P., Keller, C. A., Fritz, T. M., et al. (2021). Harmonized emissions component (HEMCO) 3.0 as a versatile emissions component for atmospheric models: Application in the GEOS-Chem, NASA GEOS, WRF-GC, CESM2, NOAA GEFS-aerosol, and NOAA UFS models. *Geoscientific Model Development*, *14*(9), 5487–5506. https://doi.org/10.5194/gmd-14-5487-2021

Liu, F., Tao, Z. N., Beirle, S., Joiner, J., Yoshida, Y., Smith, S. J., et al. (2022). A new method for inferring city emissions and lifetimes of nitrogen oxides from high-resolution nitrogen dioxide observations: A model study. *Atmospheric Chemistry and Physics*, *22*(2), 1333–1349. https://doi.org/10.5194/acp-22-1333-2022

Lorente, A., Boersma, K. F., Eskes, H. J., Veefkind, J. P., van Geffen, J., de Zeeuw, M. B., et al. (2019). Quantification of nitrogen oxides emissions from build-up of pollution over Paris with TROPOMI. *Scientific Reports*, *9*(1), 10. https://doi.org/10.1038/s41598-019-56428-5

Lu, Z., Streets, D. G., de Foy, B., Lamsal, L. N., Duncan, B. N., & Xing, J. (2015). Emissions of nitrogen oxides from US urban areas: Estimation from ozone monitoring instrument retrievals for 2005-2014. *Atmospheric Chemistry and Physics*, *15*(18), 10367–10383. https://doi.org/10.5194/acp-15-10367-2015

Luo, L., Wu, Y. F., Xiao, H. Y., Zhang, R. J., Lin, H., Zhang, X. L., & Kao, S. J. (2019). Origins of aerosol nitrate in Beijing during late winter through spring. *Science of the Total Environment*, *653*, 776–782. https://doi.org/10.1016/j.scitotenv.2018.10.306

Marais, E. A., Kelly, J. M., Vohra, K., Li, Y. F., Lu, G. D., Hina, N., & Rowe, E. C. (2023). Impact of legislated and best available emission control measures on UK particulate matter pollution, premature mortality, and nitrogen-sensitive habitats. *Geohealth*, *7*(10), e2023GH000910. https://doi.org/10.1029/2023gh000910

Marvin, M. R., Palmer, P. I., Latter, B. G., Siddans, R., Kerridge, B. J., Latif, M. T., & Khan, M. F. (2021). Photochemical environment over Southeast Asia primed for hazardous ozone levels with influx of nitrogen oxides from seasonal biomass burning. *Atmospheric Chemistry and Physics*, *21*(3), 1917–1935. https://doi.org/10.5194/acp-21-1917-2021

McDuffie, E. E., Smith, S. J., O'Rourke, P., Tibrewal, K., Venkataraman, C., Marais, E. A., et al. (2020). A global anthropogenic emission inventory of atmospheric pollutants from sector- and fuel-specific sources (1970-2017): An application of the community emissions data system (CEDS). *Earth System Science Data*, *12*(4), 3413–3442. https://doi.org/10.5194/essd-12-3413-2020

McLinden, C. A., Fioletov, V., Shephard, M. W., Krotkov, N., Li, C., Martin, R. V., et al. (2016). Space-based detection of missing sulfur dioxide sources of global air pollution. *Nature Geoscience*, *9*(7), 496–500. https://doi.org/10.1038/ngeo2724

Miyazaki, K., Eskes, H. J., Sudo, K., & Zhang, C. (2014). Global lightning NO_x production estimated by an assimilation of multiple satellite data sets. *Atmospheric Chemistry and Physics*, *14*(7), 3277–3305. https://doi.org/10.5194/acp-14-3277-2014

Murray, L. T., Jacob, D. J., Logan, J. A., Hudman, R. C., & Koshak, W. J. (2012). Optimized regional and interannual variability of lightning in a global chemical transport model constrained by LIS/OTD satellite data. *Journal of Geophysical Research*, *117*(D20), 14. https://doi.org/10.1029/2012jd017934

Pommier, M. (2023). Estimations of NO_x emissions, NO_2 lifetime and their temporal variation over three British urbanised regions in 2019 using TROPOMI NO_2 observations. *Environmental Science: Atmospheres*, *3*(2), 408–421. https://doi.org/10.1039/d2ea00086e

Pope, R. J., Kelly, R., Marais, E. A., Graham, A. M., Wilson, C., Harrison, J. J., et al. (2022). Exploiting satellite measurements to explore uncertainties in UK bottom-up NO_x emission estimates. *Atmospheric Chemistry and Physics*, *22*(7), 4323–4338. https://doi.org/10.5194/acp-22-4323-2022

Potts, D. A., Marais, E. A., Boesch, H., Pope, R. J., Lee, J., Drysdale, W., et al. (2021). Diagnosing air quality changes in the UK during the COVID-19 lockdown using TROPOMI and GEOS-Chem. *Environmental Research Letters*, *16*(5), 054031. https://doi.org/10.1088/1748-9326/abde5d

Randerson, J. T., Van Der Werf, G. R., Giglio, L., Collatz, G. J., & Kasibhatla, P. S. (2017). Global fire emissions Database, version 4.1 (GFEDv4). https://doi.org/10.3334/ORNLDAAC/1293

Shah, V., Jacob, D. J., Li, K., Silvern, R. F., Zhai, S., Liu, M., et al. (2020). Effect of changing NO$_x$ lifetime on the seasonality and long-term trends of satellite-observed tropospheric NO$_2$ columns over China. *Atmospheric Chemistry and Physics*, *20*(3), 1483–1495. https://doi.org/10.5194/acp-20-1483-2020

Sillman, S. (1999). The relation between ozone, NO$_x$ and hydrocarbons in urban and polluted rural environments. *Atmospheric Environment*, *33*(12), 1821–1845. https://doi.org/10.1016/s1352-2310(98)00345-8

Silvern, R. F., Jacob, D. J., Mickley, L. J., Sulprizio, M. P., Travis, K. R., Marais, E. A., et al. (2019). Using satellite observations of tropospheric NO$_2$ columns to infer long-term trends in US NO$_x$ emissions: The importance of accounting for the free tropospheric NO$_2$ background. *Atmospheric Chemistry and Physics*, *19*(13), 8863–8878. https://doi.org/10.5194/acp-19-8863-2019

Sun, K., Zhu, L., Cady-Pereira, K., Miller, C. C., Chance, K., Clarisse, L., et al. (2018). A physics-based approach to oversample multi-satellite, multispecies observations to a common grid. *Atmospheric Measurement Techniques*, *11*(12), 6679–6701. https://doi.org/10.5194/amt-11-6679-2018

The International GEOS-Chem User Community. (2021). GCClassic version 13.3.4 [Software]. *Zenodo*. https://doi.org/10.5281/zenodo.5764874

The International GEOS-Chem User Community. (2022). GCHP version 13.4.1 [Software]. *Zenodo*. https://doi.org/10.5281/zenodo.6564711

Tzortziou, M., Kwong, C. F., Goldberg, D., Schiferl, L., Commane, R., Abuhassan, N., et al. (2022). Declines and peaks in NO$_2$ pollution during the multiple waves of the COVID-19 pandemic in the New York metropolitan area. *Atmospheric Chemistry and Physics*, *22*(4), 2399–2417. https://doi.org/10.5194/acp-22-2399-2022

Valin, L. C., Russell, A. R., & Cohen, R. C. (2013). Variations of OH radical in an urban plume inferred from NO$_2$ column measurements. *Geophysical Research Letters*, *40*(9), 1856–1860. https://doi.org/10.1002/grl.50267

van Geffen, J., Boersma, K. F., Eskesl, H., Sneep, M., Ter Linden, M., Zara, M., & Veefkind, J. P. (2020). S5P TROPOMI NO$_2$ slant column retrieval: Method, stability, uncertainties and comparisons with OMI. *Atmospheric Measurement Techniques*, *13*(3), 1315–1335. https://doi.org/10.5194/amt-13-1315-2020

van Geffen, J., Eskes, H., Boersma, K. F., & Veefkind, P. (2021). *TROPOMI ATBD of the total and tropospheric NO$_2$ data products (issue 2.2.0)*. Royal Netherlands Meteorological Institute (KNMI), De Bilt, the Netherlands.

van Geffen, J., Eskes, H., Compernolle, S., Pinardi, G., Verhoelst, T., Lambert, J.-C., et al. (2022). Sentinel-5P TROPOMI NO$_2$ retrieval: Impact of version v2.2 improvements and comparisons with OMI and ground-based data. *Atmospheric Measurement Techniques*, *15*(7), 2037–2060. https://doi.org/10.5194/amt-15-2037-2022

Verstraeten, W. W., Boersma, K. F., Douros, J., Williams, J. E., Eskes, H., Liu, F., et al. (2018). Top-down NO$_x$ emissions of European cities based on the downwind plume of modelled and space-borne tropospheric NO$_2$ columns. *Sensors*, *18*(9), 2893. https://doi.org/10.3390/s18092893

Vohra, K., Marais, E. A., Bloss, W. J., Schwartz, J., Mickley, L. J., Van Damme, M., et al. (2022). Rapid rise in premature mortality due to anthropogenic air pollution in fast-growing tropical cities from 2005 to 2018. *Science Advances*, *8*(14), 13. https://doi.org/10.1126/sciadv.abm4435

Vohra, K., Marais, E. A., Suckra, S., Kramer, L., Bloss, W. J., Sahu, R., et al. (2021). Long-term trends in air quality in major cities in the UK and India: A view from space. *Atmospheric Chemistry and Physics*, *21*(8), 6275–6296. https://doi.org/10.5194/acp-21-6275-2021

Weng, H. J., Lin, J. T., Martin, R., Millet, D. B., Jaeglé, L., Ridley, D., et al. (2020). Global high-resolution emissions of soil NO$_x$, sea salt aerosols, and biogenic volatile organic compounds. *Scientific Data*, *7*(1), 15. https://doi.org/10.1038/s41597-020-0488-5

Wu, N., Geng, G. N., Yan, L., Bi, J. Z., Li, Y. S., Tong, D., et al. (2021). Improved spatial representation of a highly resolved emission inventory in China: Evidence from TROPOMI measurements. *Environmental Research Letters*, *16*(8), 11. https://doi.org/10.1088/1748-9326/ac175f

Yue, X., Unger, N., Harper, K., Xia, X. G., Liao, H., Zhu, T., et al. (2017). Ozone and haze pollution weakens net primary productivity in China. *Atmospheric Chemistry and Physics*, *17*(9), 6073–6089. https://doi.org/10.5194/acp-17-6073-2017

Zhang, L., Jacob, D. J., Knipping, E. M., Kumar, N., Munger, J. W., Carouge, C. C., et al. (2012). Nitrogen deposition to the United States: Distribution, sources, and processes. *Atmospheric Chemistry and Physics*, *12*(10), 4539–4554. https://doi.org/10.5194/acp-12-4539-2012